13th World Conference on Earthquake Engineering
Vancouver, B.C., Canada
August 1-6, 2004
Paper No. 2388

ANALYTICAL MODELING OF SOIL-STRUCTURE INTERACTION FOR BRIDGE COLUMNS

ChangSoon RHA[1], John W. WALLACE[2], Ertugrul TACIROGLU[3]

ABSTRACT

Cast-in-drilled-hole (CIDH) bridge shaft/columns provide an economical option for highway construction. The inelastic deformations for a CIDH shaft/column occur below grade; therefore, the overall lateral load behavior of the system is influenced by the interaction between the shaft and the surrounding soil, commonly modeled using *p-y* curves. The principal focus of this paper is on the development and verification of a robust single-degree-of-freedom model for composite *p-y* behavior. The model incorporates frictional forces (drag) and formation of gaps at the pile-soil interface, as well as inelastic soil behavior. The robustness of the model is assessed with parametric studies on various shaft/column systems and soil types.

INTRODUCTION

Cast-in-drilled-hole (CIDH) shafts (piles) typically consist of a continuous column with a prismatic cross-section. CIDH systems are common in urban regions because they do not require significant space and eliminate the complexities of a column-to-footing connection. Dynamic response of a shaft/column and the surrounding soil involves a variety of complex phenomena, including the relative motion between the shaft and the free-field soil, radiation damping, and frictional contact and gap formation at the shaft-soil interface. Although finite element models may be used to model the shaft and soil (e.g., Brown and Shie [1], Trochanis et al. [2], Brown et al. [3], Yang and Jeremic [4]), the degree of uncertainty associated with the specification of model parameters and the difficulties encountered in mesh generation and interpretation of results, often makes the application of FEM impractical. As a result, nonlinear pile-soil interaction is typically analyzed using a Winkler (beam on inelastic foundation) model, commonly referred as the "*p-y* method," where *p* denotes the soil reaction per unit length and *y* denotes the lateral shaft deflection.

The basic *p-y* method does not explicitly take into account specific aspects of the pile-soil interaction problem mentioned previously, such as gapping and drag or elastic re-loading and unloading cycles. However, it is possible to incorporate these by creating a composite single degree-of-freedom (SDOF) element, where sub-elements are used to model a particular process of the interaction, and assembled into

---

[1] Graduate Student Researcher, Univ. of California, Los Angeles, USA. Email: csrha@seas.ucla.edu
[2] Assoc. Prof., UCLA, USA. Email: wallace@seas.ucla.edu
[3] Assist. Prof., UCLA, USA. Email: etacir@seas.ucla.edu

a macro SDOF element. The assembled interaction element can then be attached to structural (beam, plate, shell) finite element models of the shaft to study the soil-structure interaction problem. Examples of this approach include interaction elements by Nogami et al. [5], who combined springs and dashpots to incorporate damping into the basic elastoplastic soil response represented by a *p-y* model. A more sophisticated model by Boulanger et al. [6] is capable of simulating the drag forces as well as the formation of gaps. Although these models are promising, details of the implementation and the ability of the model to converge for a broad range of soil and shaft properties have not been addressed. In this study, we focus precisely on these issues. The proposed interaction element is composed of a robust gap element, which provides a smooth transition between contact and no-contact phases, and elastoplastic elements, which incorporate classical rate-independent plasticity models and return-mapping algorithms. The modular and intuitive structure of the proposed element enables consideration of soil-types possessing different plastic envelope curves without altering the other aspects of the interaction. We demonstrate the robustness of the element through parametric studies involving a variety of soil response parameters and shaft boundary conditions. For brevity, the presented results are limited to response of elastic piles subjected to cyclic, quasi-static loadings; however, extensions incorporating inertial effects, inelastic pile response and radiation damping are straightforward. These are deferred to a subsequent study.

A SINGLE D.O.F. ELEMENT FOR PILE-SOIL INTERACTION

The proposed interaction element is an assembly of three distinct elements: (1) a drag element to account for friction between the shaft and the soil, (2) a gap element to account for gapping between the shaft and the soil, and (3) an elastoplastic *p-y* element to account for the hysteretic response of soil. Specific attributes of the model, as well as its unique features and implementation details are discussed in the following paragraphs. The governing equations for the drag and the *p-y* elements are based on classical rate-independent elastoplasticity [7] and the backbone curve of the *p-y* element is chosen to be identical to the *p-y* curve for (soft) clay in API [8] for the present discussion. The gap element is formulated as a projection operator that provides a smooth transition between contact and no-contact phases of deformation. It should also be noted that the three individual components (i.e., gap, drag and *p-y* elements) are assembled in a different (and arguably, more physically realistic) configuration from the earlier studies (e.g., Nogami et al. [5], Boulanger et al. [6]).

The basic elements

A schematic of the interaction element is shown in Figure 6 (right). Each component of the element is assembled in parallel to model the reaction of surrounding soil. The following sections provide the formulation of the individual components and their combined behavior.

The drag element

The drag element models the frictional forces along the pile–soil interface. Displayed in Figure 1, it possesses a single parameter (σ_d) which corresponds to the drag stress the element would generate when it is in motion. The governing equations for this element are identical to those of one-dimensional classical, rate-independent, perfect plasticity, that is:

$$\sigma = \sigma_d \ \operatorname{sign}(\dot{\varepsilon}) \tag{1}$$

where $\dot{\varepsilon}$ is the strain rate and the "signum" function is given by,

$$\operatorname{sign}(\dot{\varepsilon}) = \begin{cases} +1 & \text{if } \dot{\varepsilon} > 0, \\ -1 & \text{if } \dot{\varepsilon} < 0, \\ 0 & \text{if } \dot{\varepsilon} = 0. \end{cases} \tag{2}$$

The yield function f_d, the consistency and persistency conditions (see, for example, Simo and Hughes [7]) for the drag element, are given by:

$$f_d = |\sigma| - \sigma_d \le 0, \quad |\dot{\varepsilon}| f_d = 0, \quad \text{and } f_d = 0 \quad \Rightarrow \quad |\dot{\varepsilon}| \dot{f}_d = 0. \tag{3}$$

As such, the drag element cannot function as a load-controlled agent but is a slave element, which generates the appropriate drag forces as it deforms. For numerical robustness, a very stiff spring can be attached to the drag element in series to allow for a smoother transition between "stick" and "slip" behaviors. If properly chosen, such a spring generates only negligible amounts of elastic strain. An alternative approach is to replace the signum function of Eq. 2 by a smooth switch function. The former approach is adopted in this study as either approach yields very similar results without a significant change in robustness.

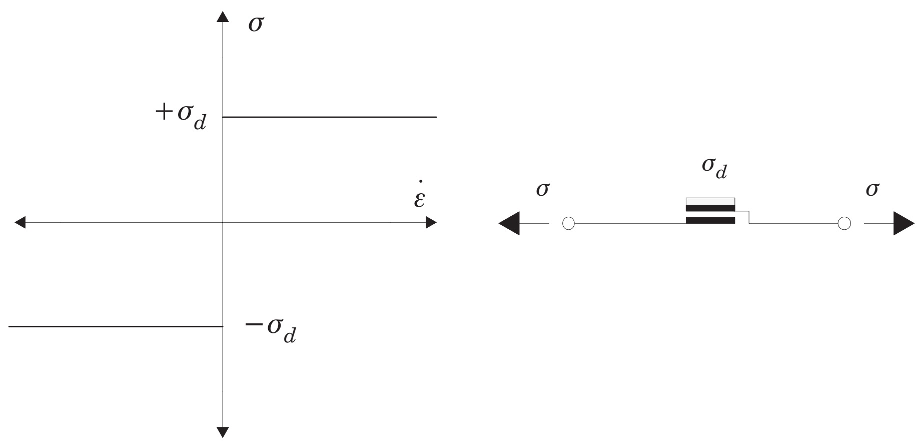

Figure 1. The drag element.

The gap element

Under cyclic loading, the pile and the soil frequently comes in and out of contact, and as a result of the inelastic deformations, gaps accrue at their interface. A robust element that enables the modeling of such contact and gapping behavior is essential for achieving convergence in numerical analyses. Strict enforcement of contact/no-contact conditions usually result into oscillatory behavior in iterative solution methods such as Newton-Raphson, and thus, a smoother transition between closed-gap and open-gap phases is generally needed to avoid convergence problems. Furthermore, due to uneven contact surfaces, a transition region may actually capture the real behavior more closely. Gap opening and closing can be achieved via a projection operator, $p(\sigma)$, which maps a perfectly transmitted stress (σ) into a stress that is transmitted through a gap. Therefore, through a perfect gap element, no stress is transmitted, i.e., $p(\sigma) = 0$, when the gap is open; and stress is perfectly transmitted, i.e., $p(\sigma) = \sigma$, when the gap is closed. The gap element proposed here possesses a single parameter (σ_L), which corresponds, conceptually, to the limit stress the element would generate in a deviation from the exact behavior. Thus, the projected stress, $p(\sigma)$, is given by,

$$p(\sigma) = \sigma - \frac{1}{2\beta}\log\left(\frac{e^{2\beta\sigma} + 1}{2}\right), \quad \beta = \frac{\log(2)}{2\sigma_L} \tag{4}$$

It follows that the rate of change of the projected stress with respect to strain, i.e., the element tangent stiffness, is:

$$\frac{\partial\, p(\sigma)}{\partial \varepsilon} = \frac{\partial p}{\partial \sigma}\frac{\partial \sigma}{\partial \varepsilon} = \frac{1}{\left(2^{\sigma/\sigma_L} + 1\right)}\frac{\partial \sigma}{\partial \varepsilon} \tag{5}$$

Furthermore, we have the limiting cases,

$$\lim_{\sigma \to +\infty} p(\sigma) = \sigma_L \qquad \lim_{\sigma \to -\infty} p(\sigma) = \sigma + \sigma_L \tag{6}$$

Figure 2 displays how the gap element would project the stress of a generic device (the X-box in Figure 2) connected to it. The sign of the parameter σ_L determines the gap direction. Without any modification to Eq. 4, $\sigma_L > 0$ or $\sigma_L < 0$ produces a limit-tension or a limit-compression response in the element, respectively. It should also be noted that the projection operator, via Eq.6, provides the tangent stiffness of any macro element (e.g., that in Figure 2) possessing a serially connected gap element in a simple fashion.

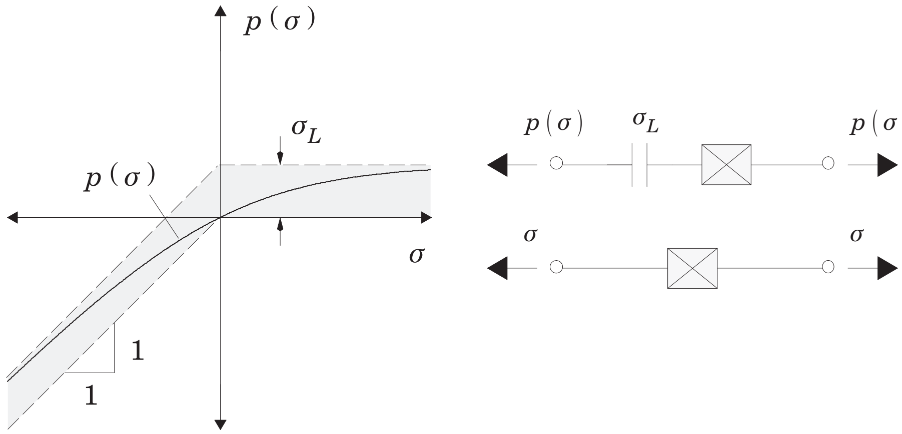

Figure 2. The gap element.

The elastoplastic p-y element for clay

The elastoplastic *p-y* element consists of a linear spring and a frictional device connected in series as displayed in Figure 3. As a consequence, the total strain admits the additive decomposition, thus:

$$\sigma = E\varepsilon^e = E\left(\varepsilon - \varepsilon^p\right) \qquad \Leftarrow \qquad \varepsilon = \varepsilon^e + \varepsilon^p \tag{7}$$

where E is the stiffness of the linear spring and ε, ε^e, ε^p are the total, elastic and plastic strains, respectively. The yield function for the frictional device is given by,

$$f_{py} = -\text{sign}\left(\sigma_L\right)\sigma - \left(\sigma_Y + \alpha\right) \le 0 \tag{8}$$

where $\sigma_Y \ge 0$ is the yield stress, $\alpha > 0$ is the hardening variable, and σ_L is an external parameter which provides the sign (or the direction) for plastic behavior. For example, if $\sigma_L < 0$ as in Figure 3, then the frictional device only yields under tensile stresses and is perfectly rigid under compression. For $\sigma_L > 0$, the opposite would be true. Thus, the elastoplastic *p-y* element never yields on the gap-side if it is connected to a gap element in series (which then provides the parameter σ_L). The evolution equations for the stress and the hardening variable (σ, α) are given by,

$$\left(\dot{\sigma}, \dot{\alpha}\right) = \begin{cases} \left(C\left(\varepsilon\right)\dot{\varepsilon}, \quad \left|\dot{\sigma}\right|\right) & \text{if } f_{py} = 0, \\ \left(E\dot{\varepsilon}, \quad 0\right) & \text{if } f_{py} < 0. \end{cases} \tag{9}$$

Consequently, the elastoplastic (continuum) material tangent stiffness is,

$$\frac{\partial \dot{\sigma}}{\partial \dot{\varepsilon}} = \begin{cases} C\left(\varepsilon\right), & \text{if } f_{py} = 0, \\ E, & \text{if } f_{py} < 0. \end{cases} \tag{10}$$

where E and $C(\varepsilon)$ are the elastic, and the plastic tangent stiffness. The envelope curves obtained from field tests (or from analytical models) may be used for the governing equation of elastoplastic *p-y* element. Here, we use the *p-y* curve for soft clay by Matlock [9] as the backbone curve of the loading-unloading cycles, which is stated in a generic form as follows:

$$\sigma = \eta \ \text{sign}\left(\varepsilon\right)\left(\frac{\left|\varepsilon\right|}{\beta}\right)^n \tag{11}$$

This gives the plastic tangent stiffness as,

$$C(\varepsilon) \equiv \frac{\eta n}{\beta^n} |\varepsilon|^{n-1} \tag{12}$$

where the material parameters η, β, n are readily available for soft clay for various depths (Matlock [9], API [8]). The yield stress σ_Y for the elastic portion is not an independent parameter and is related to the rest of the material parameters via the relation as,

$$\sigma_Y = E \sqrt[(1-n)]{\eta / (E\beta^n)} \tag{13}$$

Note that, the *p-y* curve of Matlock [9] implicitly contains the drag forces. Thus, Eq. 11 needs to be modified by an offset with the value defined in Eq. 1, in order to include the drag force without modifying the *p-y* envelope curve. Governing equations for the *p-y* elastoplastic element can be discretized and integrated via the standard "return-mapping" algorithm (Simo and Hughes [7]).

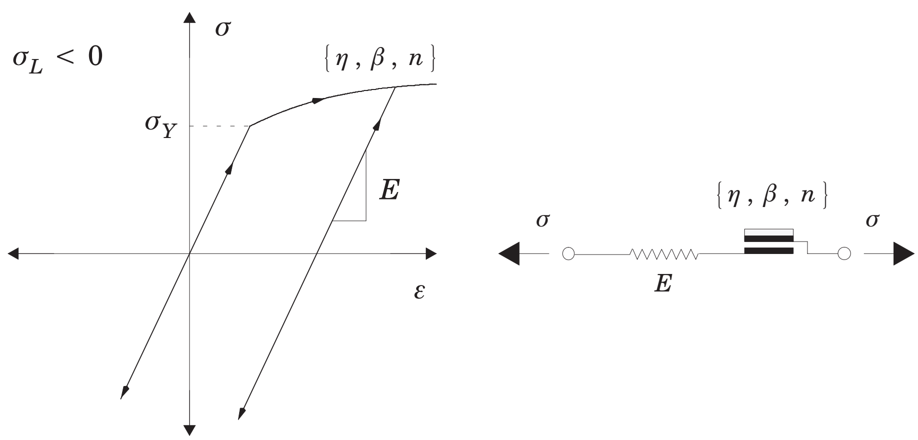

Figure 3. The *p-y* element.

Assembled intermediate elements

The basic elements are assembled to produce intermediate (sub-) elements. For example, normal and reversed gap elements are assembled with elastoplastic *p-y* elements to produce no-tension or no-compression elements that represent the soil response on either side of the pile.

The no-compression element

The no-compression element is obtained by assembling a reversed gap element and the elastoplastic *p-y* element as illustrated in Figure 4 (right). In the no-compression element, the *p-y* element behaves elastoplastically under tensile forces but behaves perfectly rigid under compressive forces.

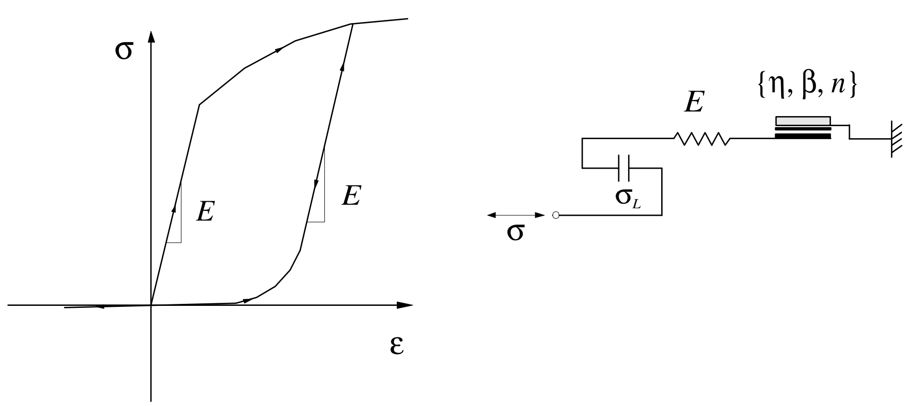

Figure 4. The no-compression element.

The reverse gap element connected in series to the elastoplastic *p-y* element coerces the compression forces below the limit stress, σ_L, which may be chosen to have a negligible value. The behavior of the no-compression element is displayed in Figure 4 (left).

The no-tension element

The no-tension element is assembled in similar manner to no-compression element. The only difference between these two is the direction of the resisting forces. The behavior of the no-tension element is displayed in Figure 5.

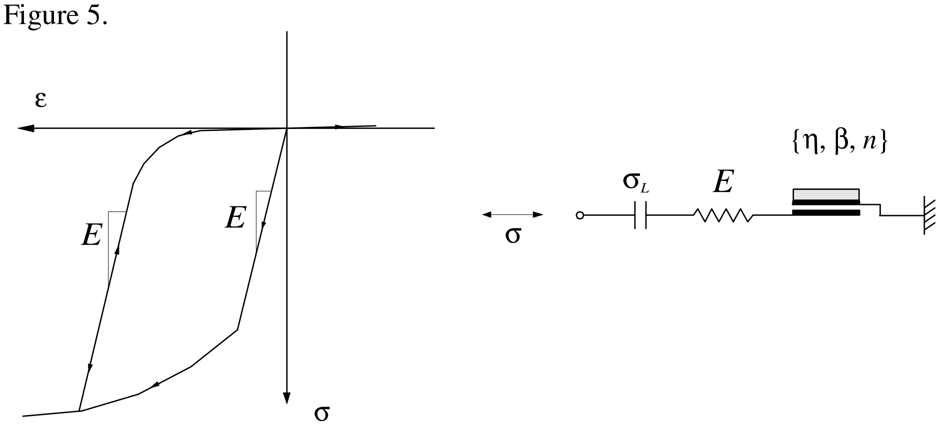

Figure 5. The no-tension element.

The combined interaction elements

The interaction element is assembled with the no-compression subelement, no-tension subelement, and the drag element in parallel. These combined interaction elements are connected to the embedded structure such as a pile, a drilled shaft, or columns on one side, as shown in Figure 7. The no-tension subelement models the compressive resistance of the leading face of the embedded structure while the no-compression element models the tensile resistance in rear face of the structure. Once the loading is reversed under cyclic loading, the no-tension element first elastically unloads and then disengages as the gap opens. Subsequently, the no-compression element starts being loaded.

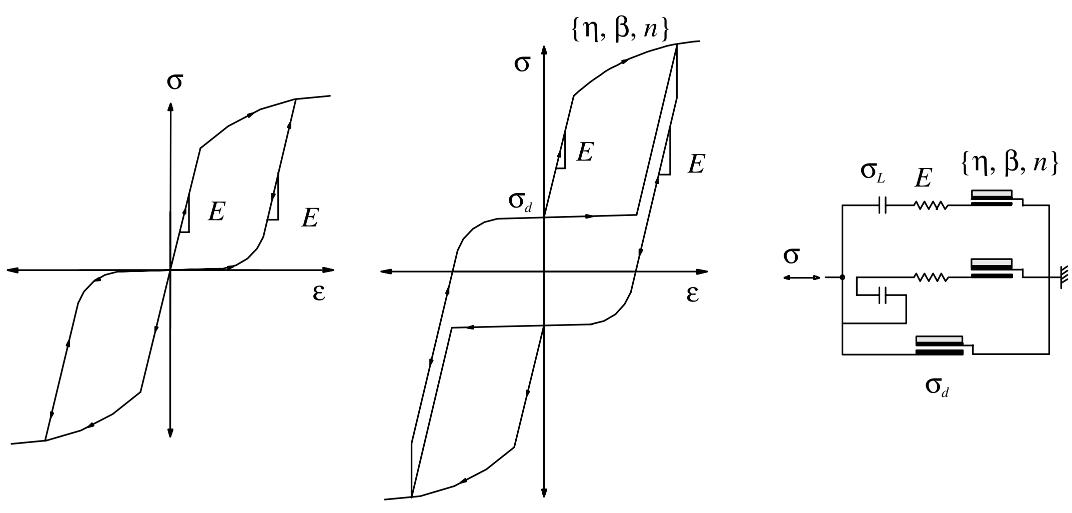

Figure 6. The interaction element (left: without drag, middle: with drag).

The drag element provides the frictional force that acts at the surface of the embedded structure. The rationale for connecting the drag element in parallel is due to the assumption that the frictional forces are always in effect while the pile is in motion. This is an additional resistance over the no-tension or no-compression element. The behavior of the combined interaction element is displayed in Figure 6 with and without consideration of drag resistance.

THE NUMERICAL EXAMPLES

Two numerical examples with extensions from an earlier study (Taciroglu et al. [10]) are provided to verify the robust interaction model subjected to the cyclic loads. In the first example, a 12m long pile/shaft is embedded in clay and a cyclic lateral load is applied at the top node as illustrated in Figure 7. The pile/shaft head is fixed for rotation to mimic the behavior of a pile with a cap. The second example is the so-called flagpole shaft that is commonly used in highway bridge construction. The flagpole shaft is 15m long with 12m embedded into the clay as illustrated in Figure 7(a). Unlike the fix-headed pile, the flagpole shaft is a conditionally stable structure, i.e., the pile becomes unstable as the lateral loading reaches the limit point of lateral resistance of the surrounding soil. This happens when the stiffness of all of the interaction elements becomes zero concurrently, due to large inelastic soil deformation and/or gapping along the entire length of the shaft. Here we have used an additional spring element at the top of the pile/shaft as displayed in Figure 7(b) to avoid unstable structural response. A displacement-controlled analysis method (such as the arc-length continuation method) can be used to obtain the post-peak response without difficulty. The “net applied load” is obtained by evaluating the difference between the external force and the reaction force in the spring element at the top of the pile.

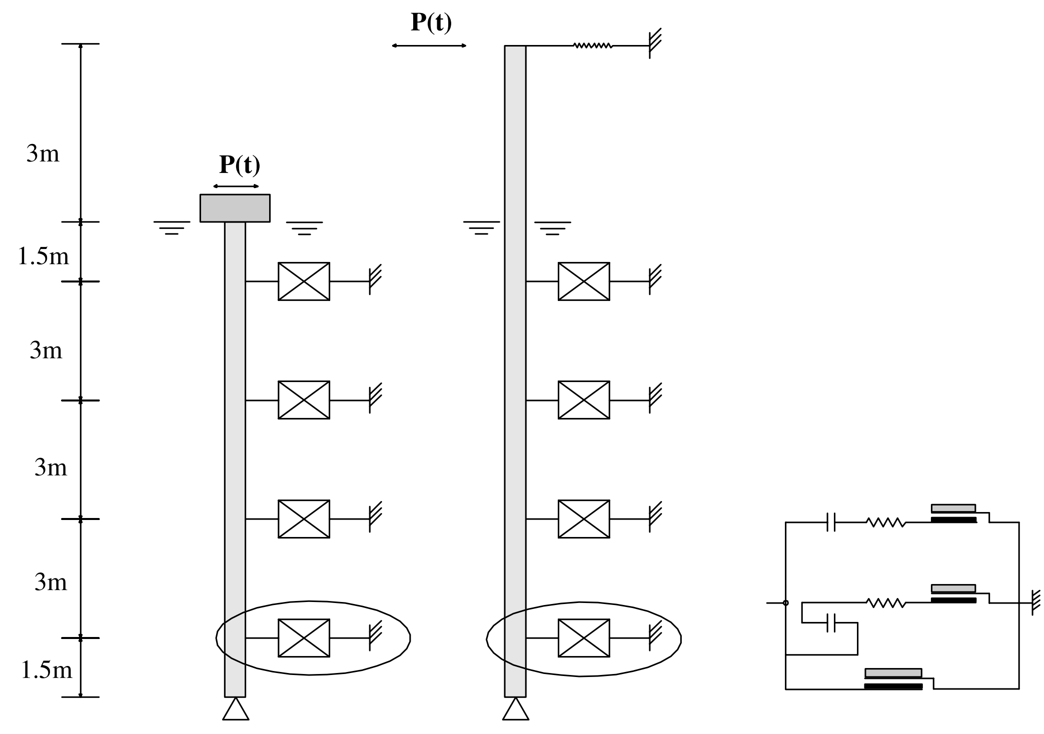

(a) Fix-headed pile model (b) Flagpole pile model (c) Interaction element

Figure 7. The example models.

The diameter of shafts in the provided examples is chosen as 1.5m. The pole is divided into 5 beam elements and these are connected to 4 interaction elements with 3.0m spacing. The bottom node is hinged (z = -12m) and the top node (z = 0m for fix-headed and z = 3m for flagpole) is subjected to a cyclic external load *P(t)* given by the expression,

$$P(t) = P_0 \sin(\omega_1 t)\sin(\omega_2 t), \quad t \in [0, \pi] \tag{14}$$

where ω_1 = 0.25, and ω_2 = 4.0. The parameter P_0 is chosen to be proportional to the total resistance of the interaction element as $P_0 = C\sqrt{\sum_{i=1}^{noi}(P_u)_i^2}$ where C is the load ratio over the resistance, P_u is the ultimate resistance of each interaction element, and *noi* denotes the number of interaction elements.

The soil is assumed to be clay; therefore, the *p-y* envelope is Matlock's curve for clay [9], which is parameterized with the undrained shear strength *c*, unit weight of the soil *γ*, pile/shaft diameter *D*, empirical constant *J*, and depth.

The pile/shaft is assumed to be elastic with a Young's modulus of E = 20,000 MPa (2,900 ksi). To verify the robustness of the interaction element, a wide range of clay properties are considered. In the examples provided here, only the undrained shear strength *c* is varied while other soil parameters such as unit weight, and the empirical constant *J* are held constant. The unit soil weight *γ* is assumed to be 19 kN/m^3 (0.07 lb/in^3), the empirical factor *J* is taken as 0.5. The shear strength *c* is categorized into three groups: soft clay (c < 25 kPa), medium clay (c = 25~50 kPa), and stiff clay (c = 50~100 kPa) as described in Coduto [11]. The values of shear strength for each category are chosen as 10 kPa, 50 kPa, and 100 kPa, respectively. These properties are summarized in Table 1.

Table 1. Material parameters for the interaction elements

c (kPa)	z (m)	p_u (kN/m)†	η (kN)	β (m)‡	E (kN/m)	σ_d (kN)
10	-1.5	95.25	142.9	.0375	3,810	57.2
	-4.5	195.75	293.6	.0375	7,830	117.4
	-7.5	296.25	444.4	.0375	11,850	177.8
	-10.5	396.75	595.1	.0375	15,870	238.0
50	-1.5	305.25	457.9	.0375	12,210	183.2
	-4.5	465.75	698.6	.0375	18,630	279.4
	-7.5	626.25	939.4	.0375	25,050	375.8
	-10.5	786.75	1,180.1	.0375	31,470	472.0
100	-1.5	567.75	851.6	.0375	22,710	340.6
	-4.5	803.25	1,204.9	.0375	32,130	482.0
	-7.5	1,038.75	1,558.1	.0375	41,550	623.2
	-10.5	1,274.25	1,911.4	.0375	50,970	764.6

$^\dagger\, p_u = \left(3 + \frac{\gamma z}{c} + \frac{Jz}{D}\right) cD \qquad ^\ddagger\, \beta = y_c = 2.5\varepsilon_c D$

The material constants in Table 1 are obtained through Matlock's [9] description of the *p-y* curves. Consequently, the equivalencies $\eta = 0.5 \times p_u \times L_{tr}$, $\beta = y_c$ hold between Matlock's parameters and the parameters used here. The parameter n in Eq. 11 through Eq. 13 is taken as 1/3. The strain ε_c, which occurs at one-half of the maximum stress on the laboratory stress-strain curve, is assumed to be 0.01 for the evaluation y_c. The elastic loading/unloading modulus is chosen to be $E = \eta/\beta$, similar to the initial modulus used by Matlock [9]. The tributary length for each of the pile-soil interaction elements is L_{tr} = 3.0m. The parameter μ is the ratio of the drag force to the ultimate resistance, thus drag stress becomes $\sigma_d = 2.0\ \eta\ \mu$. As the drag force is implicitly included in the original *p-y* curves in Matlock's [9] and API [8], it is inserted here such that the elastoplastic *p-y* envelope of the API formulation remains unaltered.

The numerical analysis of two examples with all of the chosen parameters yielded convergent results uniformly, verifying the numerically robustness of the soil-structure interaction element and its amenability for routine structural analysis. In all the computations performed, convergence was achieved without the use of any safeguarding algorithm such as line searches or sub-incrementation techniques. Table 2 displays the summarized response quantities for the two examples.

Table 2. Various response quantities for the numerical examples

Pile/shaft Type	Response Quantities	Soft (c =10 kPa)	Medium (c = 50 kPa)	Stiff (c = 100 kPa)
Fix-headed	Max. Peak Load (kN) †	5,161	10,968	18,280
	Max. Top Disp. (mm)	417.7	825.9	1,342.5
	Max. Gap (mm) ‡	569.6	1,203.6	2,015.7
Flag-pole	Max. Peak Load (kN) †	948	2,089	3,527
	Max. Top Disp. (mm)	372.6	466.8	572.6
	Max. Gap (mm) ‡	296.2	348.3	408.5

† Applied net load (e.g., applied load minus the reaction force in spring for the flagpole). The load ratio C is chosen as 5.0 for the fix-headed shaft and 1.0 for the flagpole, respectively.

‡ Measured at the depth of the 1st interaction element, i.e. at z = -1.5m.

A variety of response quantities for the fix-headed pile/shaft are provided in Figures 8 through 10. Those for the flagpole are provided in Figures 11 through 13. For the sample responses provided in plots in Figures 8 through 13, the shear strength of soil was c=50 kPa and the drag ratio was 20%. Figures 8 and 11 display the top displacement of the pile/shaft and the lateral deflection versus lateral pressure, i.e. *p-y* curves at the depth of each interaction element. Figures 9 and 12 display the magnitude of the gaps at the same depths. Figures 10 and 13 display the moment and displacement distributions along the shaft at each peak load. As expected, the magnitude of inelastic deformations and the gaps reduce as the depth increases.

CONCLUSIONS

The objective of this study has been the development of a reliable and computationally efficient model for the embedded piles/shafts under lateral loads. The newly formulated interaction element is numerically robust and amenable to routine structural analysis as convergence in nonlinear equilibrium iterations is achieved for a wide range of soil properties. In subsequent studies, this interaction element will be used in simulating the response observed in field tests (Wallace et al. [12]) that were performed on a CIDH bridge shaft (as well as in additional tests that are planed). In contrast to the API experiments, these field tests were performed on large diameter, reinforced concrete shafts under cyclic loading with sustained damage to the shafts at various locations. All these additional attributes have been observed to have a significant impact on the observed behavior. In subsequent studies, we will undertake the development of novel *p-y* curves suitable for large diameter shafts through comparisons of response observed in field tests, and those predicted in simulations using the interaction elements developed in this study.

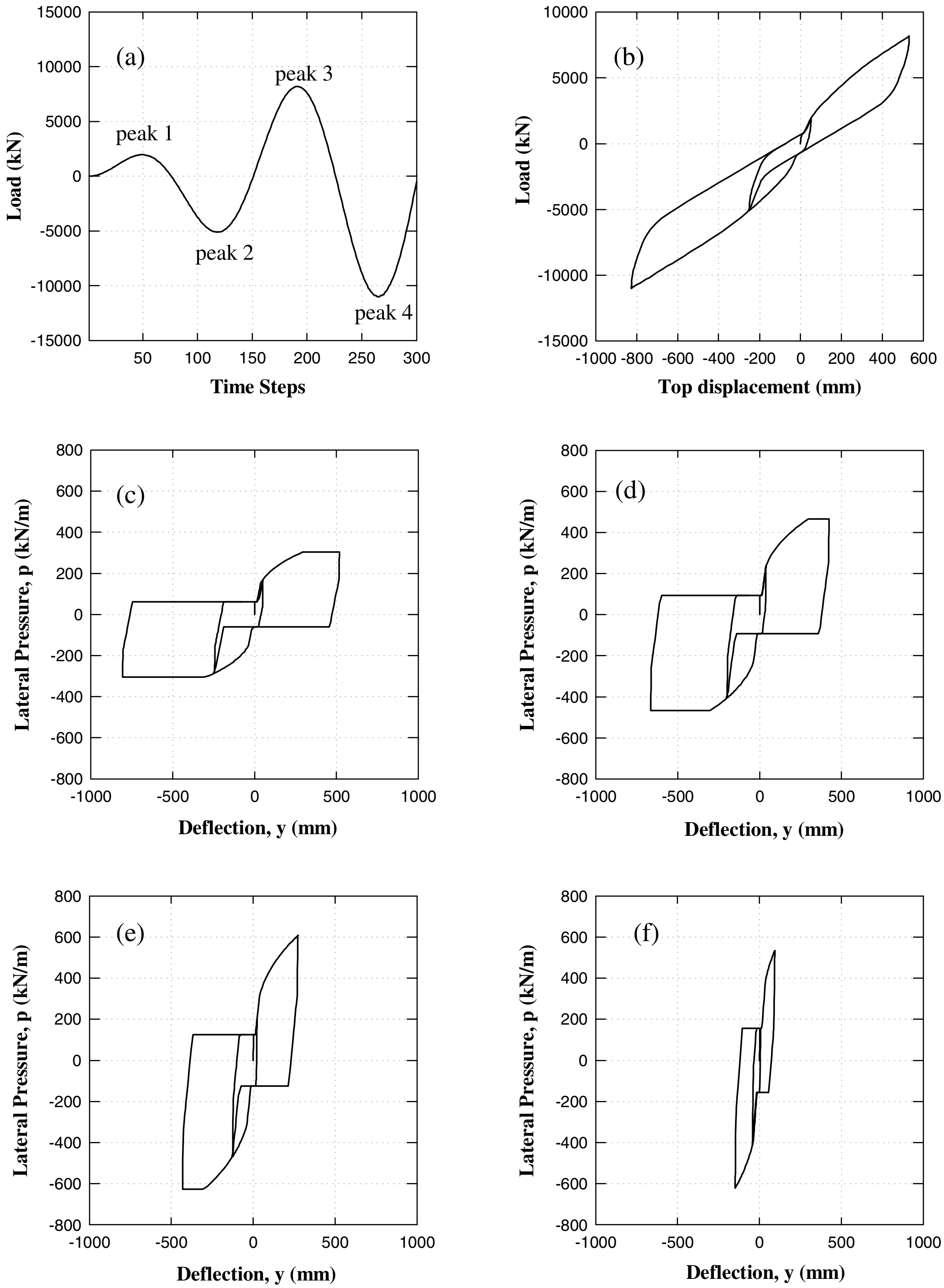

Figure 8. Response quantities for the fix-headed pile: (a) applied load, (b) displacement at the shaft top, (c, d, e, f) *p-y* curve at depths, -1.5m, -4.5m, -7.5m, -10.5m, respectively.

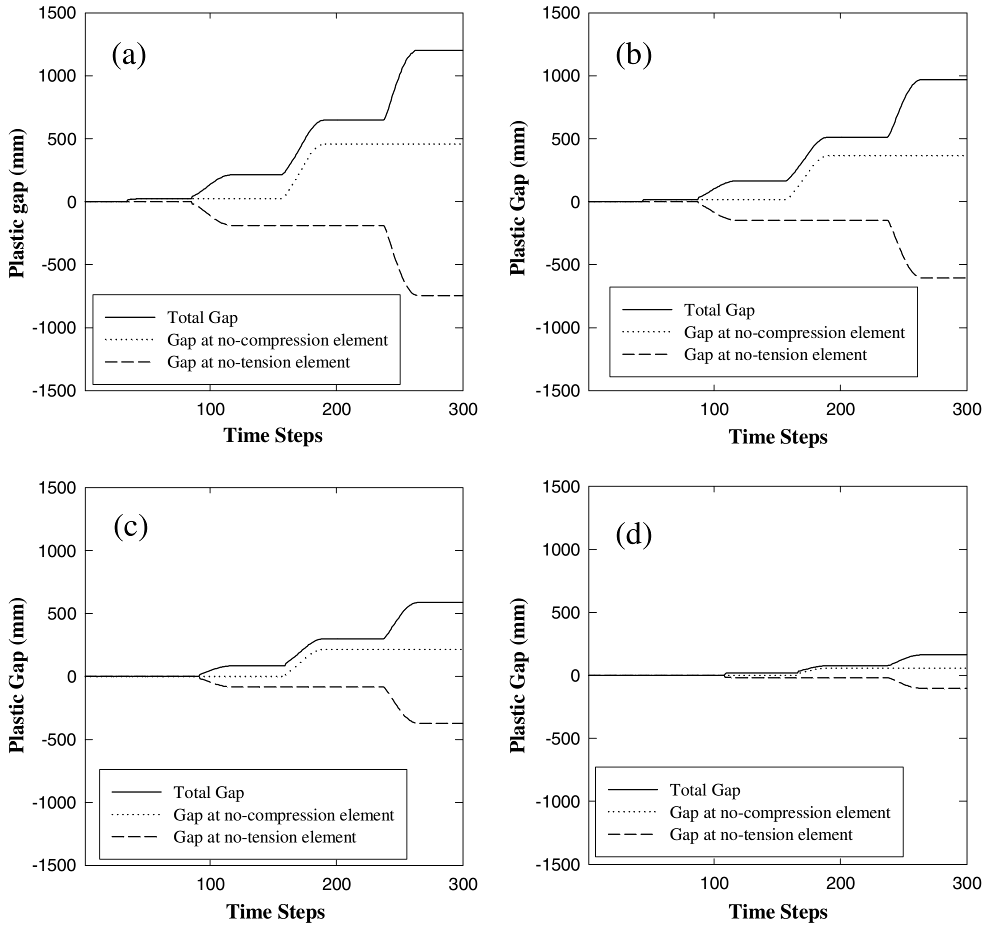

Figure 9. Response quantities for the fix-headed pile: (a, b, c, d) gap opening at depths, -1.5m, -4.5m, -7.5m, -10.5m, respectively.

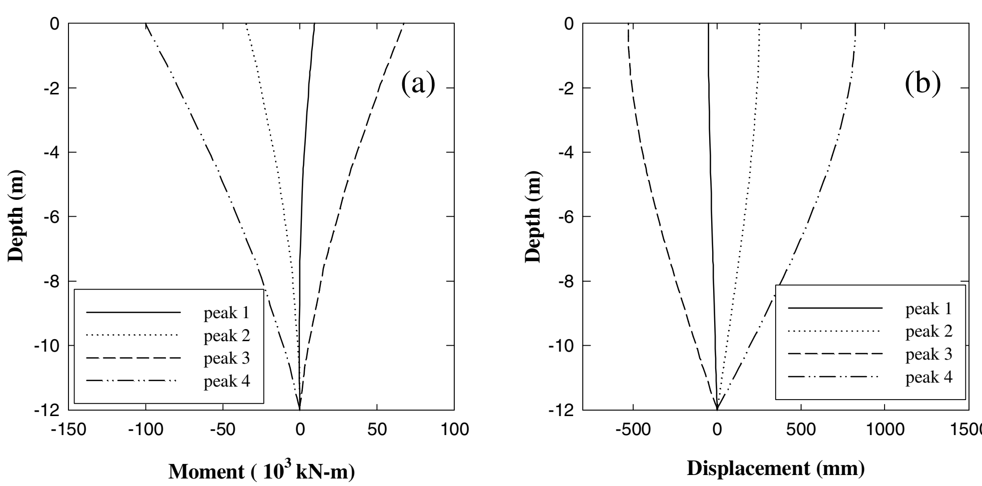

Figure 10. Response quantities for the fix-headed pile: (a) moments, and (b) displacements along the pile at peak loads.

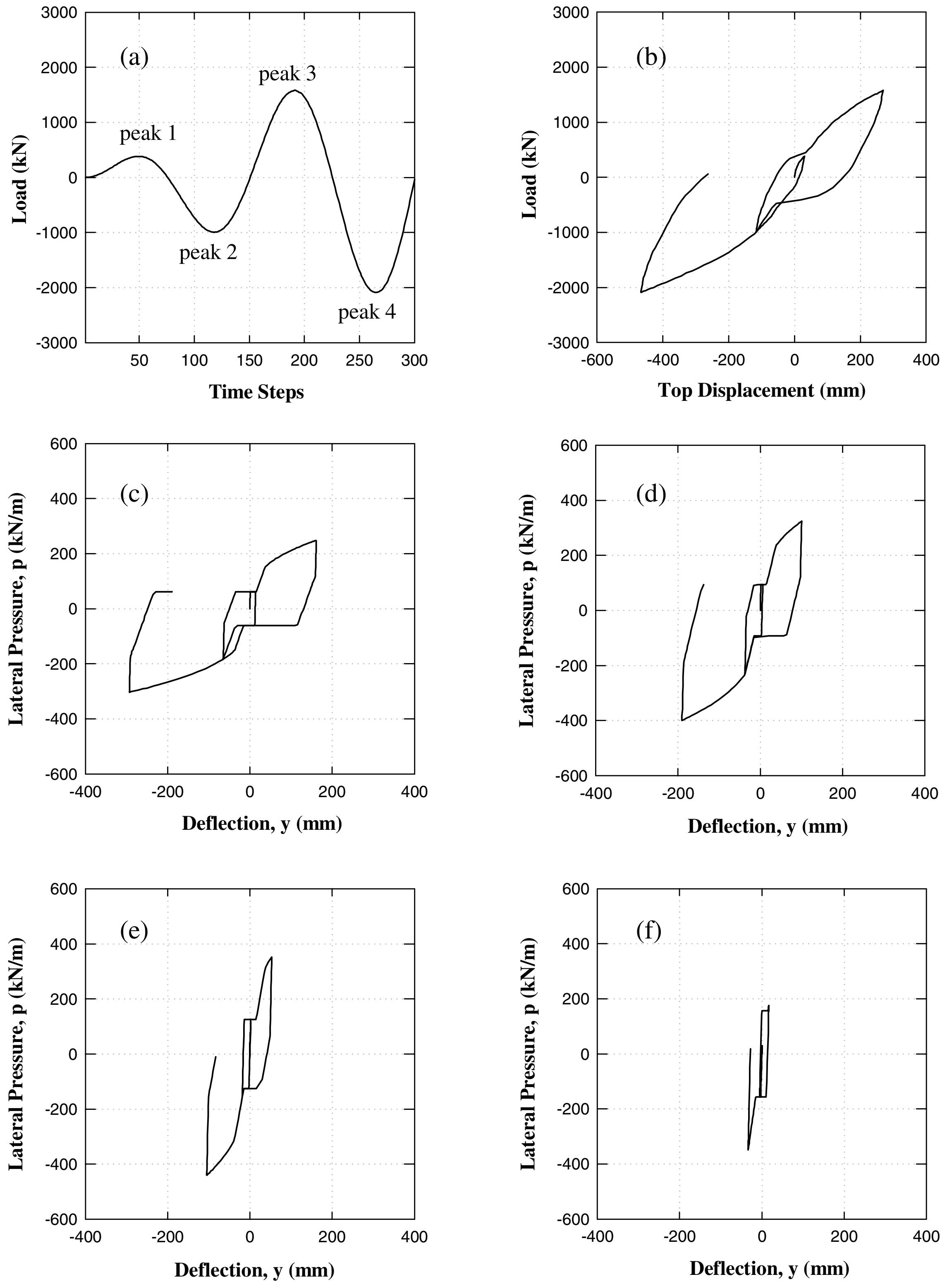

Figure 11. Response quantities for the flagpole: (a) applied (net) load, (b) displacement at the shaft top, (c, d, e, f) *p-y* curve at depths, -1.5m, -4.5m, -7.5m, -10.5m, respectively.

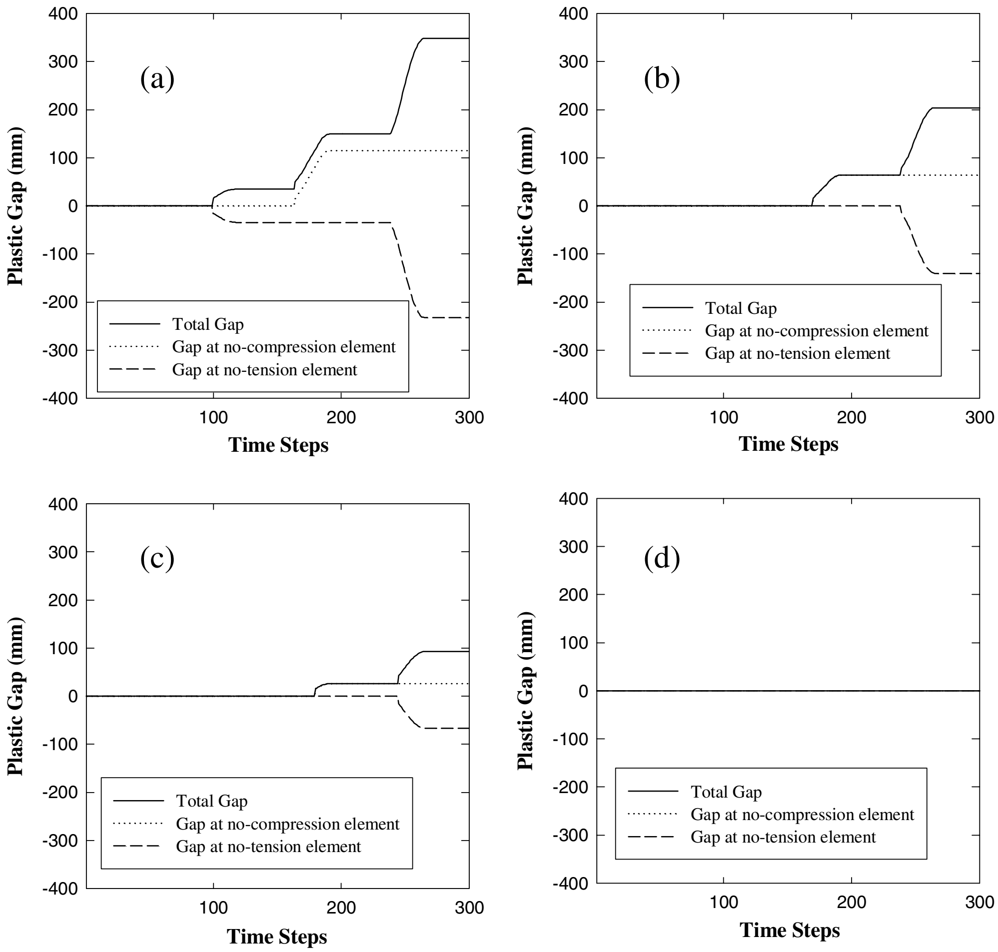

Figure 12. Response quantities for the flagpole: (a, b, c, d) gap opening at depths, -1.5m, -4.5m, -7.5m, -10.5m, respectively.

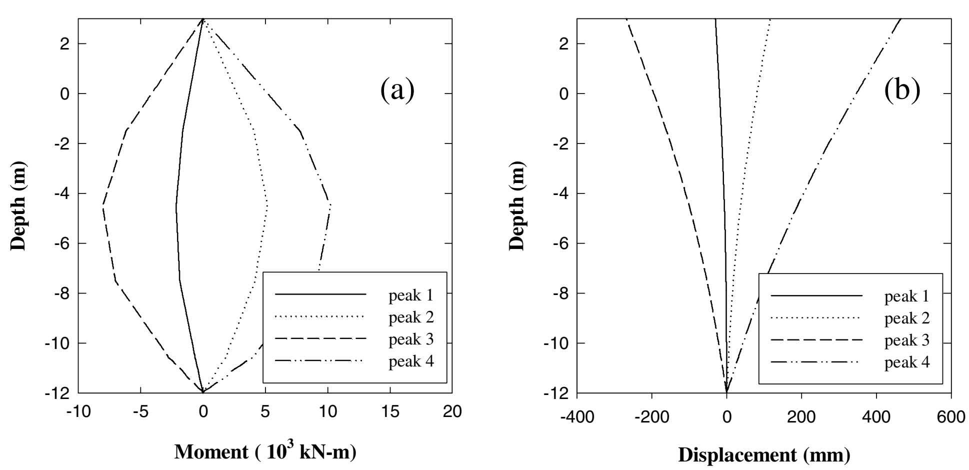

Figure 13. Response quantities for the flagpole: (a) moments, and (b) displacements along the pile at peak loads.

ACKNOWLEDGMENT

This project was funded by the Caltrans under contract number 59A0247. The support and comments of Caltrans engineers, Craig Whitten and Anoosh Shamsabadi are greatly appreciated. The contents of this paper do not necessarily represent a policy of Caltrans.

REFERENCES

1. Brown D, and Shie CF. “Some Numerical Experiments with a Three Dimensional Finite Element Model of a Laterally Loaded Pile.” Computers and Geotechnics, ASCE, 1991; 12: 149-162.
2. Trochanis A, Bielak J, Christiano P. “Three-dimensional Nonlinear Study of Piles.” Journal of the Geotechnical Engineering Division, ASCE, 1991; 117(3): 429-447.
3. Brown D, Shie CF, Kumar M. “P-Y Curves for Laterally Loaded Piles Derived from Three Dimensional Finite Element Model.” Proceeding of 3rd International Symposium on Numerical Models in Geomechanics, Niagara Falls, 1989: 683-690.
4. Yang Z, Jeremic B. “Numerical Analysis of Pile Behaviour under Lateral Loads in Layered Elastic-Plastic Soils.” International Journal for Numerical and Analytical Methods in Geomechanics, 2002; 26: 1385-1406.
5. Nogami T, Otani J, Konagai K, Chen HL. “Nonlinear soil-pile Interaction Model for Dynamic Lateral Motion.” Journal of the Geotechnical and Geoenvironmental Engineering, ASCE, 1992; 118(1): 89-106.
6. Boulanger RW, Curras CJ, Kutter BL, Wilson DW, Abghari A. “Seismic Soil-Pile-Structure Interaction Experiments and Analyses.” Journal of Geotechnical and Geoenvironmental Engineering, ASCE, 1999; 125(9): 750-759.
7. Simo JC, Hughes TJR. “Computational Inelasticity” Vol. 7 of Interdisciplinary Applied Mechanics, Springer, New York, 1988.
8. American Petroleum Institute “Recommended Practice for Planning, Designing, and Constructing Fixed Offshore Platforms – Working Stress Design.” Report RP2A-WSD, 20th Edition, 1993.
9. Matlock H. “Correlations for Design of Laterally Loaded Piles in Soft Clay.” Proceedings of the 2nd Offshore Technology Conference, Houston, 1970, OTC 1204; 1: 577-594.
10. Taciroglu E, Rha CS, Stewart JP, Wallace JW. “Robust Numerical Models for Cyclic Response of Columns Embedded in Soil.” 16th ASCE Engineering Mechanics Conference, University of Washington, Seattle, 2003.
11. Coduto DP. “Foundation Design. Principles and Practices, 2nd Edition” New Jersey: Prentice Hall, 2001.
12. Wallace JW, Fox PJ, Stewart JP, Janoyan K, Qiu T, Lermitte S. “Cyclic Large Deflection Testing of Shaft Bridges.” Report to the California Department of Transportation, University of California, Los Angels, 2001, Part 1: 1-168.